Differential roles of high gamma and local motor potentials for movement preparation and execution

Aysegul Gunduz, Peter Brunner, Mohit Sharma, Eric C. Leuthardt, Anthony L. Ritaccio, Bijan Pesaran & Gerwin Schalk

View supplementary material

Submit your article to this journal

View related articles

Citing articles: 3 View citing articles

Published online: 04 May 2016.

View Crossmark data

Taylor & Francis
Taylor & Francis Group

Differential roles of high gamma and local motor potentials for movement preparation and execution

Aysegul Gunduz[a]*, Peter Brunner[b,c], Mohit Sharma[d], Eric C. Leuthardt[e], Anthony L. Ritaccio[c], Bijan Pesaran[f] and Gerwin Schalk[b,c]

[a]*J. Crayton Pruitt Family Department of Biomedical Engineering, University of Florida, Gainesville, FL, USA; [b]National Center for Adaptive Neurotechnologies, Wadsworth Center, NY State Department of Health, Albany, NY, USA; [c]Department of Neurology, Albany Medical College, Albany, NY, USA; [d]Department of Biomedical Engineering, Washington University, St. Louis, MO, USA; [e]Department of Neurosurgery, Washington University, St. Louis, MO, USA; [f]Center for Neural Sciences, New York University, New York, NY, USA*

Determining a person's intent, such as the planned direction of their movement, directly from their cortical activity could support important applications such as brain-computer interfaces (BCIs). Continuing development of improved BCI systems requires a better understanding of how the brain prepares for and executes movements. To contribute to this understanding, we recorded surface cortical potentials (electrocorticographic signals; ECoG) in 11 human subjects performing a delayed center-out task to establish the differential role of high gamma activity (HGA) and the local motor potential (LMP) as a function of time and anatomical area during movement preparation and execution. High gamma modulations mostly confirm previous findings of sensorimotor cortex involvement, whereas modulations in LMPs are observed in prefrontal cortices. These modulations include directional information during movement planning as well as execution. Our results suggest that sampling signals from these widely distributed cortical areas improves decoding accuracy.

Keywords: brain-computer interfaces; BCI; electrocorticography; ECoG; sensorimotor systems

I. Introduction

Brain-computer interface (BCI) research develops neurotechnologies that enable people to interact with brain activity, and thereby supports entirely new avenues for diagnosis or treatment of neuromuscular or neurological disorders.[1] For example, BCI devices can support robot-assisted neurorehabilitation,[2,3] or brain-based control of arm prostheses [4,5] or wheelchairs.[6–9] BCI research experienced impressive growth over the past two decades, and instigated some of the most dynamic and far-reaching multidisciplinary collaborations of our time. Some of the most important BCI approaches use brain signals that have relationships with particular parameters of movements. However, the differential role of different brain signal components and their ability to predict movement direction in different areas of the brain have remained unclear.

To contribute to understanding in this area, we aimed to verify and more fully characterize the spatiotemporal processes that prepare for and execute directional movements in human electrocorticographic (ECoG) signals. ECoG signals combine high spatial resolution with high temporal resolution, and demonstrate negligible susceptibility to other physiological artifacts.[10,11] Together with its apparent superior long-term stability,[12,13]

ECoG should be well suited to satisfy the complex demands of clinically viable BCIs.[14] In our study, we asked 11 human subjects to engage in a center-out task [15] using a joystick with eight possible targets while we recorded ECoG signals using subdurally placed electrodes. These electrodes can detect power modulations at high frequencies (>70 Hz, high gamma activity (HGA)) that cannot readily be detected in scalp recordings. These modulations reflect asynchronous local activity in the cortex rather than synchronized cortical rhythms.[16] Results from many studies demonstrated that HGA is highly correlated with different types of behavior [17] and thus is a prime candidate to support BCI applications.[14,18,19] In addition, time-domain variations in ECoG signals called local motor potentials (LMP,[20–22] also called low-frequency components, LFC [23]), have also been shown to modulate with movements and thus are likely to be relevant to BCI systems.

The objectives of the study were to: (i) establish the differential role of HGA and LMP activity as a function of time and anatomical area during movement preparation and execution; (ii) examine and compare the amount of directional information from these two ECoG features; (iii) investigate the impact of the number of electrodes sampled across cortical areas and ECoG features on the

---

accuracy of the decoded directional information in single trials. Our results confirm and extend previous findings by showing that movement-related ECoG responses are found in a highly distributed network that involves the premotor, parietal, and prefrontal cortices.[5,24,25] Sampling from these distributed regions improves decoding accuracy of the direction of movement preparation and execution in single trials. The results also highlight the differential role of HGA and LMP as a function of time and anatomical area during movement preparation and execution. HG activations are observed in the premotor and parietal areas during movement preparation and in the primary motor areas during execution, whereas LMP activations are observed the dorsolateral prefrontal cortex during movement preparation and execution, and with sensorimotor cortex activations during execution.

II.   Materials and methods

A.   Human subjects and cortical models

Eight subjects at Albany Medical Center and three subjects at Washington University at St. Louis participated in this study. The study was approved by the Institutional Review Boards of both hospitals as well as by the Human Research Protections Office of the US Army Medical Research and Materiel Command. All subjects gave informed consent. Subjects were patients with intractable epilepsy who underwent temporary placement of subdural electrode arrays to localize seizure foci prior to surgical resection. The implanted electrode grids (Ad-Tech Medical Corp., Racine, WI) consisted of platinum-iridium electrodes that were 4 mm in diameter (2.3 mm exposed), spaced at an inter-electrode distance of 10 mm, and were embedded in silicone. Subject H was implanted with a custom high-density temporal grid with an inter-electrode distance of 6 mm (PMT Corp, Chanhassen, MN) (see Figure 1). Electrode contacts distant from epileptic foci and areas of interest were used for reference and ground. The number of implanted electrodes varied between 58 and 111 contacts across subjects. The electrode numbers and a summary of the subjects' clinical profiles are given in Table 1. Nine subjects underwent grid implantation over the left hemisphere, whereas two subjects' implants were placed on the right hemisphere (Subjects D and E).

We established three-dimensional cortical models of individual subjects using pre-operative structural magnetic resonance imaging (MRI) using Curry software (Compumedics, Charlotte, NC). We then co-registered these MRI images with post-operative computer tomography (CT) images, transformed the result into the Talairach coordinate system,[26] and identified electrode locations from the CT images using Curry software. The resulting cortical models and electrode localizations are presented in Figure 2. We accounted for brain surface shifts (e.g., due to craniotomy) by projecting the electrodes onto the convex hull of the cortical model using the NeuralAct software.[27] We also assigned these electrode locations to Brodmann areas using the Talairach Daemon (http://www.talairach.org [28]). Finally, we generated cortical activation maps using the NeuralAct software utilizing the 3D cortical model that was derived from the respective subject. For activation maps that were computed across subjects, electrode positions from each patient were projected to the three-dimensional cortical template provided by the Montreal Neurological Institute (MNI) (http://www.bic.mni.mcgill.ca). Note that for the visualization of accumulated activity across subjects, we projected the grid implants of Subjects D and E (whose electrodes were implanted on the right hemisphere) to the left hemisphere.

Neuropsychological evaluations (Wechsler Adult Intelligence Scale-III) revealed low average to superior motor performance (25th–99th percentile) as well as average to superior visuomotor scanning performance and visual search capacity (37th–91st percentile) across patients. Subjects had corrected-to-normal vision and did not suffer from any visual impairment. The subjects had performance IQs of at least 85 and were mentally and physically capable of performing the task.

B.   Data collection

The experimental setup is depicted in Figure 3. We recorded ECoG signals at the bedside using eight 16-channel g.USBamp biosignal acquisition devices (g.tec, Graz, Austria) at a sampling rate of 1200 Hz. In addition to recording brain activity, we also recorded the subjects' eye gaze using a monitor with a built-in eye-tracking system (Tobii Tech., Stockholm, Sweden) positioned 54–60 cm in front of the subjects, and the activity from a push button. The built-in sampling rate of the eye tracker was 60 Hz. Eye tracker data were upsampled to 1200 Hz by sample-and-hold (i.e. no interpolations between two samples from the eye tracker). The eye tracker was calibrated to each subject at the beginning of the experimental session using custom software. Data collection from the biosignal acquisition devices, stimulus presentation, and behavioral variables (i.e. eye tracker, push button), as well as control of the experimental paradigm, were accomplished simultaneously using BCI2000 software.[29,30]

C.   Experimental paradigm

ECoG signals were collected while the subjects performed an eight-target center-out cursor movement task [31] while fixating their eye gaze at a central fixation
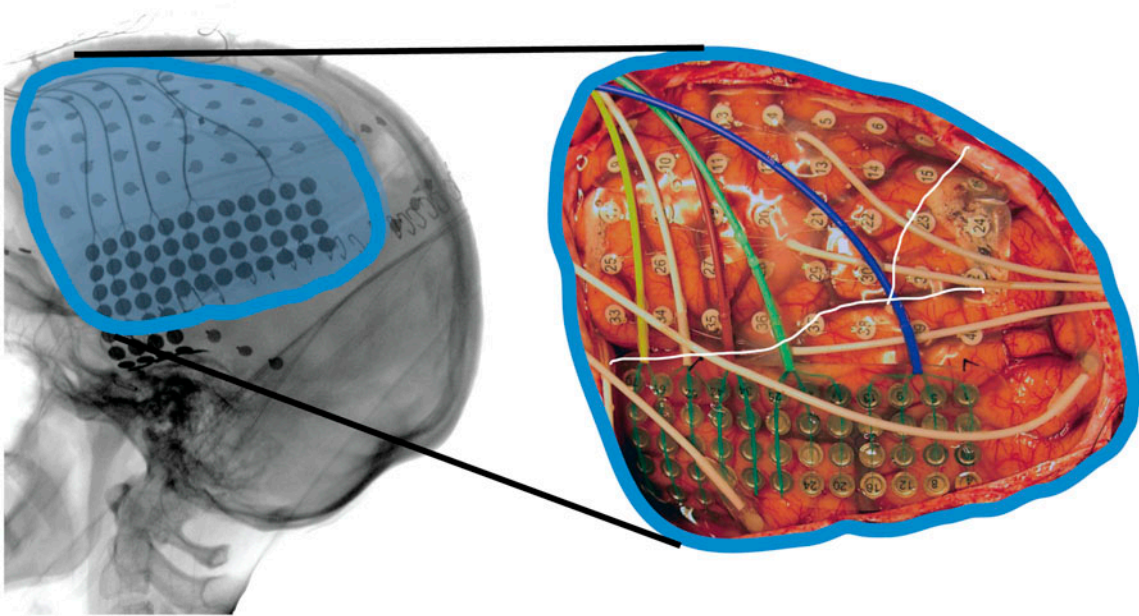
Figure 1. Subdural frontal and high density temporal clinical grid implants shown for Subject H. Left: post-operative X-ray. Right: intra-operative photograph of the implants.

cross as illustrated in Figure 3. Eye gaze fixation was confirmed online by BCI2000 and the eye tracker: a trial was aborted if the subject looked away from the center for more than 500 ms. Each trial started with the presentation of a target in one of eight possible locations. A cursor appeared 1 s later at the center of the screen. The subjects' task was to use their hand contralateral to the implants to control a joystick so as to move the cursor into the target. Thus, subjects D, E, and G used their non-dominant hands. We positioned the subjects such that the joystick movements were mainly restricted to the wrist.[20] The subjects were instructed to make exaggerated movements and achieve maximal radial extension of the joystick to hit the targets. Once the target was hit, the next trial started after an inter-trial interval of 1 s. Figure 4 gives an illustration of the stages of the task. Trials aborted by the eye tracker, trials in which joystick movement preceded the presentation of the cursor, and trials in which subjects failed to hit the correct target were omitted from further analyses. The total number of trials run per subject was a minimum of 400 trials, and the average number of remaining valid trials was 371 ± 88 across the subjects. The average reaction time and time to complete a trial for the subjects were 0.51 ± 0.21 s and 1.40 ± 0.29 s, respectively. A trial was aborted if the target was not hit 2 s after cursor presentation. The task accuracy, reaction time, and time to hit the target were not significantly different across the subjects who used their dominant hands versus the subjects who used their non-dominant hands.

D. Feature extraction

Our data analyses began with the inspection and removal of channels that were heavily affected by electrical artifacts (e.g., due to bad electrode contacts) or epileptiform activity. The channels that passed visual inspection were high-pass filtered above 0.01 Hz (using a Butterworth filter in the forward and backward directions for zero-phase delay) and re-referenced to a common average reference (CAR).[20] High gamma activity (HGA) and local motor potentials (LMP) at time t_n were computed in $[t_n - 150$ ms $t_n + 150$ ms] windows with a step window size of 100 ms ($t_{n+1} = t_n + 100$ ms). We computed power spectral density using a maximum entropy autoregressive model [31] of order 25 between 1 and 200 Hz in 1 Hz bins with linear detrending. HGA was estimated by averaging the spectral amplitudes in the 70–110 Hz (broadband) range to avoid 60 Hz line noise and its harmonics. LMP were computed from the moving average of the high-pass filtered and re-referenced signals in the same windows.

E. Decoding of movement preparation and execution

A block diagram of the task is presented in Figure 4. Herein, we aim to study the modulations in HGA and LMP during movement preparation and execution. Inter-trial periods were labeled as 'rest,' and periods after the target presentation up to the cursor presentation (i.e., the go cue) were labeled as 'movement preparation.' The beginning of the 'movement execution' period was

Table 1. Clinical profiles of participants.

Subject	Age	Sex	Handedness	Full-scale IQ / performance IQ	Seizure focus	Grid locations (number of contacts)
A	29	F	R	122 / 136	Left temporal	Left fronto-parietal (64) Left temporal (23) Left temporal pole (4) Left occipital (6)
B	56	M	R	84 / 87	Left temporal	Left frontal (56) Left temporal (35) Left occipital (6)
C	26	M	R	102 / 100	Left temporal	Left frontal (64) Left temporal (35) Left frontal pole (6) Left parietal (6)
D	25	M	R	99 / –	Right frontal	Right frontal (64) Right orbital (6) Right frontal pole (6) Right anterior mesial (6) Right mid-mesial (4) Right posterior mesial (6)
E	25	M	R	116 / 114	Right frontal	Right frontal (64) Right posterior frontal (20) Orbital superior frontal (4) Right frontal parietal (4) Right anterior mesial (4) Right posterior mesial (4)
F	45	M	R	97 / 99	Left temporal	Left frontal (54) Left temporal (4)
G	49	M	L	97 / 99	Left temporal	Left temporal frontal (61) Left temporal mesial (4) Left frontal (4)
H	25	M	R	84 / 95	Left temporal	Left frontal (64) Left anterior temporal (8) Left inferior frontal (6) Left anterior interhemispheric (8) Left anterior subtemporal (4) Left posterior subtemporal (4) Left middle inter hemispheric (6)
I	56	M	R	116 / 125	Left temporal	
J	46	M	R	– / –	Left temporal	Left frontal (56) Left temporal (35) Left occipital (6)
K	40	M	R	104 / 110	Left temporal	Left temporal inferior frontal (64) Left posterior subtemporal (16) Left anterior temporal (8) Left anterior subtemporal (4) Left suboccipital (6) Left posterior occipital (8)

defined as the time sample when the joystick was pushed beyond one-eighth of its maximum radial extension from its rest position. First, we built classifiers based on HGA and LMP features to differentiate task states (movement preparation/execution) from rest. We also studied the contribution of each feature at each electrode location and each time window to investigate the spatiotemporal evolution of the activations. We then focused on the temporal significance of the electrodes placed over motor, dorsolateral prefrontal, and temporal cortices for a comparison between HGA and LMP features.

One second of ECoG features from the beginning of each state (movement preparation/execution) were used to build the state decoders. Decoders for the movement preparation and execution states were built by considering the two corresponding binary classification problems: movement preparation versus rest, and movement execution versus rest. For each of the binary classification problems, we built three decoders: (i) HGA features alone, (ii) LMP features alone, and (iii) both features. Each decoder output was the weighted summation of 1s of ECoG features (i.e., 10 features per second of HGA
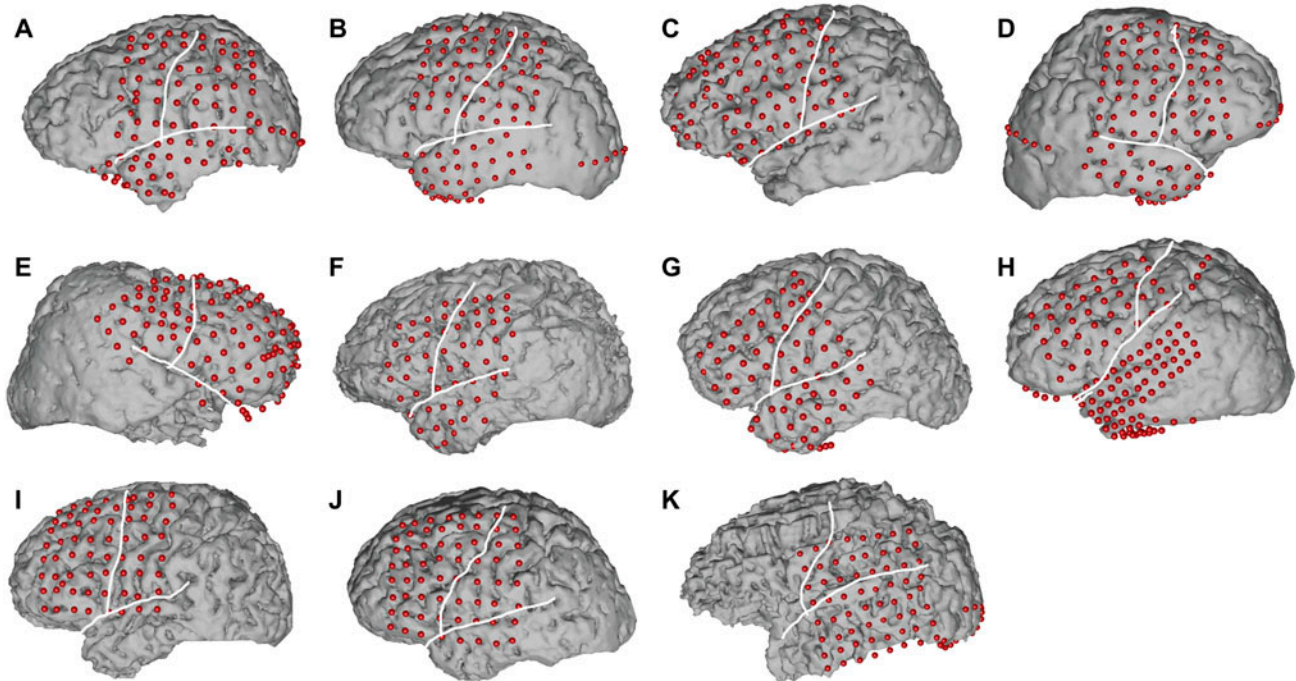
Figure 2.   Cortical models and electrode locations for all 11 subjects created from pre-op MRI and post-op CT scans.
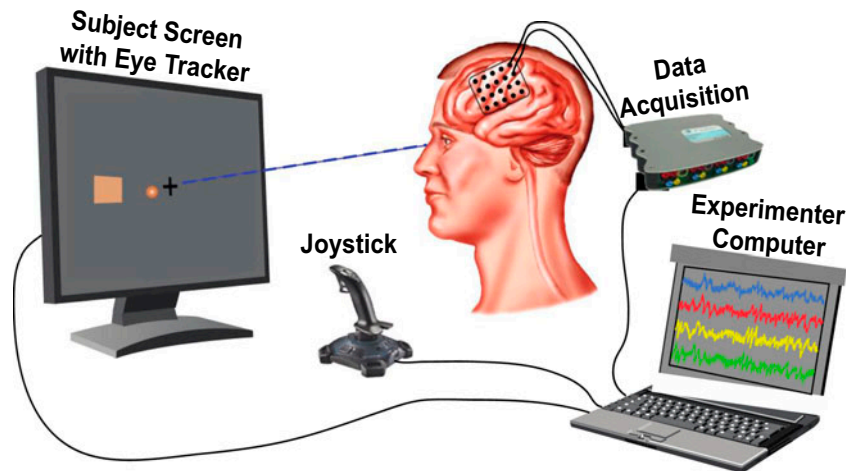

Figure 3.   Experimental setup.

and/or LMP features) across all channels. Linear weights for these binary classification problems were obtained with the stepwise multilinear regression method (SWLDA), which determined the weights of the linear function that minimized the squared error between the output estimates and labels of the classes. The decoder training and test sets were selected repeatedly in a 10-fold cross-validation procedure: the data were divided into 10 parts, and each tenth was used as the test set in turns for a classifier that was trained on the remaining 9 tenths. The accuracies corresponding to the 10 test sets

were averaged and reported. Electrodes over visual cortex were not used in the decoders to minimize any potential immediate impact of visual stimulation.

In addition, we performed univariate analyses, for each channel and each time point, to determine the spatiotemporal significance of the HGA and LMP features over cortical areas across the stages of the task. We further investigated the time evolutions of the significance of electrodes grouped over the motor, dorsolateral prefrontal, and temporal cortices for a comparison between HGA and LMP through multivariate analyses. Similar to
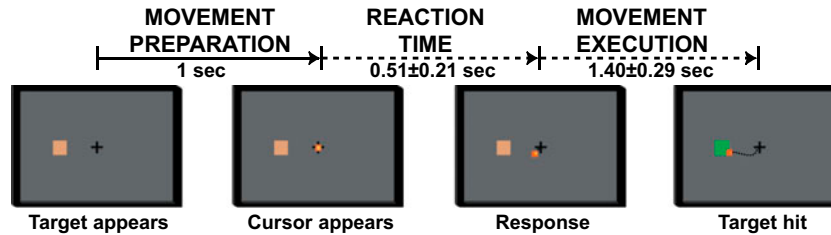
Figure 4. Experimental paradigm: (i) target appears in one of eight possible locations; (ii) a second later, a cursor appears as a go cue; (iii) subject initiates movement; (iv) subject hits the target to end the trial. Note that the time between target and cursor presentations is labeled the 'Intention' period and the time from movement initiation until the task is completed is labeled the 'Movement' period.

the analyses described above, we performed these two analyses using stepwise multilinear regression and 10-fold cross-validation procedures. For both univariate and multivariate analyses, we computed the significance by calculating the negative logarithm of the *p*-value of the correlation between the decoder outputs and true classes. Finally, we conducted the same analyses using the amplitude in the mu (8–12 Hz) and beta (18–30 Hz) frequency bands. The results suggested much lower classification accuracies than for HGA and LMP features, and thus are not presented in the following sections.

F. Decoding of movement direction

In addition, we built classifiers to decode the direction of the target during movement preparation and execution states using the HGA and LMP features. A feature selection stage was found necessary and 25% of trials were used for feature selection (not further used in training of the decoders). We plotted tuning curves by binning the feature values across these trials as a function of the eight directional angles separated by 45°. To determine whether a curve was tuned to a direction, we calculated a tuning index measure [20] calculated as the ratio of variance of features across all directions, to the average of variances of features in each direction. If, for instance, a curve is not tuned to a particular direction (i.e., the feature amplitude does not show some relationship to direction), the variance of each direction is likely to be the same as the overall variance, which will yield a tuning index that will be close to 1. The tuning index will be greater than 1 if there are some directional bins whose mean value is much higher than the rest and/or if the variance within bins is small. To determine the significance level of the tuning index, we performed surrogate analyses by shuffling the features randomly across bins and attaining the tuning index for randomly assigned bins. We repeated this procedure for 200 surrogate sets, and then derived the significance (*p*) value of our tuning index by performing a Wilcoxon signed rank test of the original measure

across the 200 surrogate measures (The test hypothesis was the distribution of surrogate values had a mean that was smaller than the original measure, which was not rejected.) The significance level of tuning for a channel was computed using false discovery rate (FDR) control to correct for multiple comparisons. We projected the accumulated negative logarithm of the significant *p*-values on MNI cortical models. (For visualization purposes, all electrodes were projected onto the left hemisphere.)

In a similar fashion to the procedure described in Cogan et al., [33] we then pooled the directionally tuned electrodes across all subjects for each feature, for a total of *N* electrodes. The minimum number of valid trials for each direction common to all significant electrodes was used during pooling to control for variability in trial numbers across subjects. For each subject, these trials were taken from the remaining 75% of trials not used previously in feature selection. The features were pooled together as though they were collected during the same experimental session. This means that given a target direction, one trial was selected across all significant electrodes and pooled to generate the features for that direction and for that trial. Thus, this pooling procedure does not increase the number of trials, but increases the number of features assigned to a trial and its corresponding target direction. We then studied the effect of the number of pooled channels, *n*, used in the decoder on classification performance. Using a total number of electrodes from $n = 1$ to N, we used a maximum of 100 permutations of *n* electrodes ($\min\{P(N,n),100\}$) to decode direction during the movement preparation and execution periods. The *n* electrodes at each iteration were selected randomly without regard to the subject labels. For each iteration, decoding of target direction was performed using linear discriminant analysis (LDA) classifiers in 10 cross-validation folds at both states of the task (movement preparation and execution). The results of all analyses are presented next. Classifiers for mu and beta bands implemented in the same manner did not result in statistically significant decoding performance.

III. Results

The relationship between the brain signals and task states is shown in Figure 5 for Subject A in three exemplary channels over the visual (top), premotor (middle), and primary motor (top) cortices. The time-frequency plots are averaged across all trials, divided by baseline activity and presented in linear scale (i.e., a scale of 1 denotes no change from baseline). Although activity from the visual cortex is not used in the decoders, herein we show the response of the visual cortex to the different stages of the experiment as captured through electrocorticography. The visual cortex electrode displays increases at frequencies higher than 50 Hz when the target and cursor are presented (top left panel). These are followed by decreased amplitude in lower frequencies, including the alpha band. Increases at 50–100 Hz are observed as the cursor moves towards the target (top right panel). Similar event-related increases in HGA and decreases in the mu band are present in premotor cortex (middle row). In primary motor cortex (bottom row), event-related decreases in mu and beta ranges accompany premotor decreases in the mu band (bottom left panel). However, HGA does not increase until the movement starts (bottom right panel). Our selection of the high gamma range (70–110 Hz) follows these observations, which are consistent across subjects, and also omits 60 Hz line noise and its harmonics.

A. Decoding movement preparation and execution from cortical activity

The main results of this analysis are presented in Table 2. This table gives the classification accuracies for discriminating movement preparation and execution from the resting state for each subject (binary classifications), averaged across 10 cross-validation folds. Using LMP features, the mean classification accuracy and its standard deviation across subjects was $85 \pm 12\%$ for detecting movement intention and $80 \pm 9\%$ for detecting hand movement (both at a 50% chance level). With HGA features, the mean classification accuracy and its standard deviation across subjects was $77 \pm 7\%$ for detecting movement intention and $82 \pm 6\%$ for detecting hand movement. Overall, across subjects, the LMP feature yielded higher classification for decoding preparation, whereas HGA yielded higher accuracy for execution. For Subject C and the LMP feature, our procedure could not detect a difference between movement intention and the rest state at the $p = .05$ level, or a difference between movement intention and the rest state at the $p = .01$ level. Furthermore, using all features for classification failed significance at $p = .01$ for decoding intention. The mean classification accuracy and its standard deviation across subjects was $79 \pm 8\%$ for detecting movement intention and $82 \pm 8\%$ for detecting hand movement when both HGA and LMP features were used.
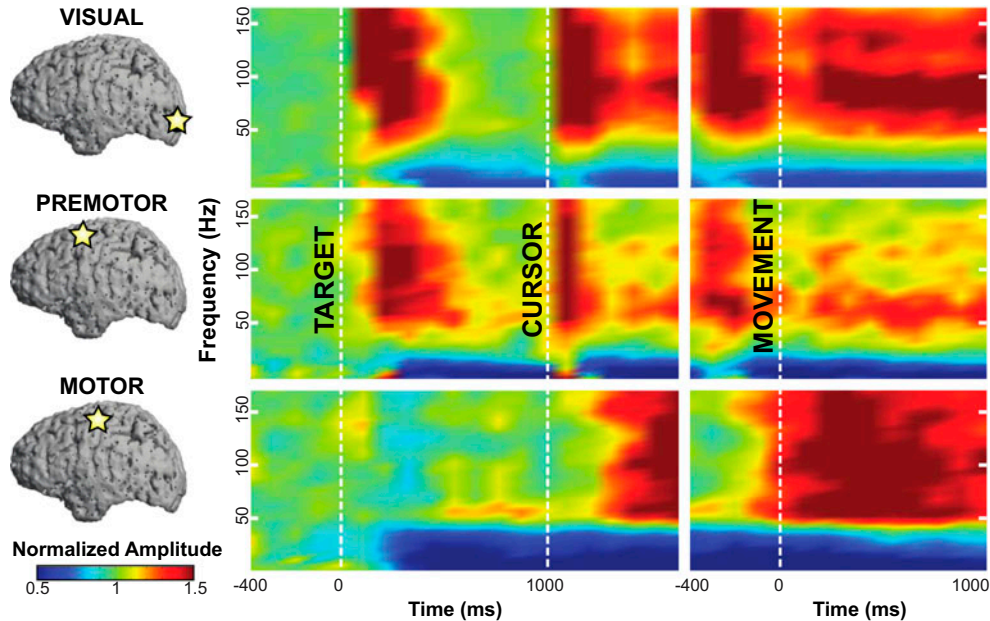

Figure 5. Left: exemplary electrodes selected over visual, premotor and primary motor cortices (top to bottom) in Subject A. Middle: spectral amplitude modulations over selected channels normalized to rest. Dashed lines indicate the onset of target and cursor presentations. Right: spectral amplitude modulations aligned to movement onset as defined by joystick extensions beyond one-eighth of maximal joystick extension range. (Note that the electrodes over the visual cortex were excluded from all subsequent quantitative analyses.)

Table 2.   Classification accuracies (mean ± standard deviation) for discriminating movement preparation and execution from rest.

	Movement preparation			Movement execution		
Subject	High gamma activity	Local motor potentials	Both	High gamma activity	Local motor potentials	Both
A	87±6%	95±3%	88±4%	91±10%	84±6%	96±3%
B	82±5%	94±2%	83±3%	85±4%	90±2%	84±3%
C	62±8%[†]	55±12%[‡]	62±9%[†]	70±6%	61±6%[†]	66±9%
D	68±10%	70±6%	69±6%	73±5%	77±6%	75±6%
E	84±4%	89±3%	84±5%	85±4%	70±9%	82±4%
F	81±6%	89±4%	82±4%	81±3%	86±5%	83±4%
G	79±5%	90±3%	79±6%	84±3%	92±3%	87±3%
H	79±5%	91±5%	83±3%	85±3%	83±6%	88±5%
I	77±10%	90±2%	80±5%	78±5%	71±5%	80±5%
J	73±7%	80±6%	75±8%	81±5%	79±5%	80±6%
K	79±4%	88±4%	81±4%	84±5%	86±6%	86±3%

[†]Failed binomial test at a confidence level of 99%.
[‡]Failed binomial test at a confidence level of 95%.

Subsequently, we were interested in determining the temporal significance of cortical locations involved in differentiating movement preparation and execution from resting states. To this end, we computed the correlations and corresponding p-values between the tasks and outputs of models for each feature at every time point for each electrode location. For each electrode, we defined a significance index as the $-\log(p)$ value. These significance indices were then accumulated for all subjects and projected onto the template MNI brain. Figure 6 depicts the spatiotemporal evolution for HGA (top panel) and LMP (bottom panel). The activations reflect the significance of the underlying area from which the features were extracted. For the three rows of each feature, 0 ms denotes time alignment around target presentation (top row), cursor presentation (middle row), and movement onset (bottom row), respectively from top to bottom. For HGA most activations are in the sensorimotor and parietal cortices, whereas activations for LMP are in the sensorimotor and prefrontal areas. To compare the two features across time, we accumulated all electrodes across subjects from the motor (Brodmann areas 4 and 6) and dorsolateral prefrontal (DLPFC; Brodmann areas 9 and 46) cortices. Figure 7 depicts the temporal evolutions of the features across these areas. The shaded areas show the standard deviation of the significance across subjects. As a control, we also accumulated electrodes from the temporal cortex, which did not show any significance for either feature at any stage of the task (red curves). For HGA motor cortex yielded higher significance than the dorsolateral prefrontal cortex. The activity in the motor cortex peaked around 400–500 ms after target presentation and increased again after cursor presentation. Activity increases with movement and peaks within ~200 ms of movement initiation. Activity in the DLPFC is much lower and is mostly focused around movement initiation. LMP seems to be equally significant in both areas.

The LMP activity in the motor cortex follows the timing of the HGA feature. LMP activation in the DLPFC, however, starts early on during the movement preparation period.

B. Decoding of direction of movement

Figure 8 shows the cortical areas for HGA and LMP that are significantly tuned to a target direction. HGA features are localized over premotor and primary hand motor cortices with some tuned channels in parietal regions. LMP features are widely distributed over the motor cortex, as well as DLPFC. For both features, cortical allocations are broader and more significant during movement execution compared to the preparation period. Out of 642 channels that had frontal and parietal cortical coverage in 11 subjects, the number of HGA channels that are significantly tuned are 18 and 20 channels during movement preparation and execution, respectively. These electrodes are marked in blue in the right panel of Figure 9. For the LMP, the significant electrode totals were 17 and 20 channels, for the two conditions, shown in red in Figure 9. Two electrodes were significantly tuned for both features during intention, and three during movement (shown in half red and blue in Figure 9). These electrodes were used in the decoding of direction.

Table 3 shows the average magnitude of the angular error of classification of movement direction in individual subjects and for movement preparation or execution, and for high gamma and local motor potentials, respectively. Across subjects, the median angular error was between 62° and 70°. Angular errors shown in bold are statistically lower than errors expected by chance (112.5°, $p = .05$). To establish statistical significance, we created 100 surrogates for each of the four cases by shuffling the classifier outputs and computed the error for the surrogates. We then compared the actual angular errors with the error distribution of the surrogates using
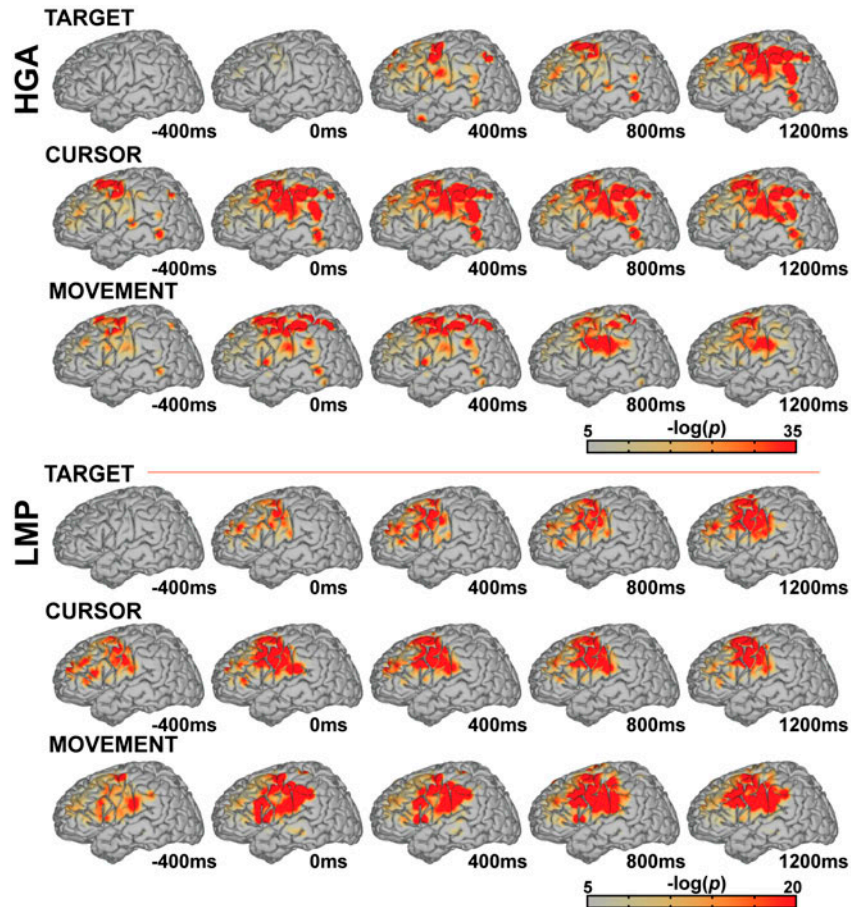
Figure 6. Temporal evolution of significant areas for discriminating tasks (movement preparation or execution) from rest accumulated across all subjects. Top panel: high gamma activation time aligned to target (top), cursor (middle), and movement (bottom) onsets. Bottom panel: local motor potential time aligned to target (top), cursor (middle), and movement (bottom) onsets.

a two- distribution *t*-test. Only two of the 11 subjects did not hold any significant directional information.

While electrodes from individual subjects only weakly encoded directional information, features pooled across subjects yielded classification accuracies significantly higher than chance level (12.5%). Average classification accuracies and the standard errors are plotted in Figure 9 as a function of number of electrodes used in the decoder. Overall, classification accuracies increase with the number of electrodes added to the LDA classifier. This result suggests that different locations encode different information about the direction of intended or executed movements. The only exception is the LMP features during intention, for which the classification results follow a stable trend just higher than chance level. When both features are used in classification, they do not perform better than HGA, but classification continues to increase with increasing number of electrode locations. Figure 10 shows the absolute error angle of classification for HGA and LMP features when all tuned

channels were utilized. In this figure, 0° corresponds to correct classification. An error angle of 45° means that the target was mistaken for one of its neighbors. Figure 10 demonstrates that the target was most frequently misclassified as one of its neighbors.

IV. Discussion

In the present study, we investigated in detail directional movement planning and execution using ECoG signals in 11 human subjects, and established the degree to which ECoG HGA and LMP features hold different information about these tasks in single trials. We localized the features that showed the most robust temporal or spectral changes during the center-out task and presented their temporal evolution. Both HGA and LMP features showed pronounced changes in the hand motor areas during movement preparation and execution, with changes in parietal regions with HGA, and in prefrontal areas with LMP (Figure 6).
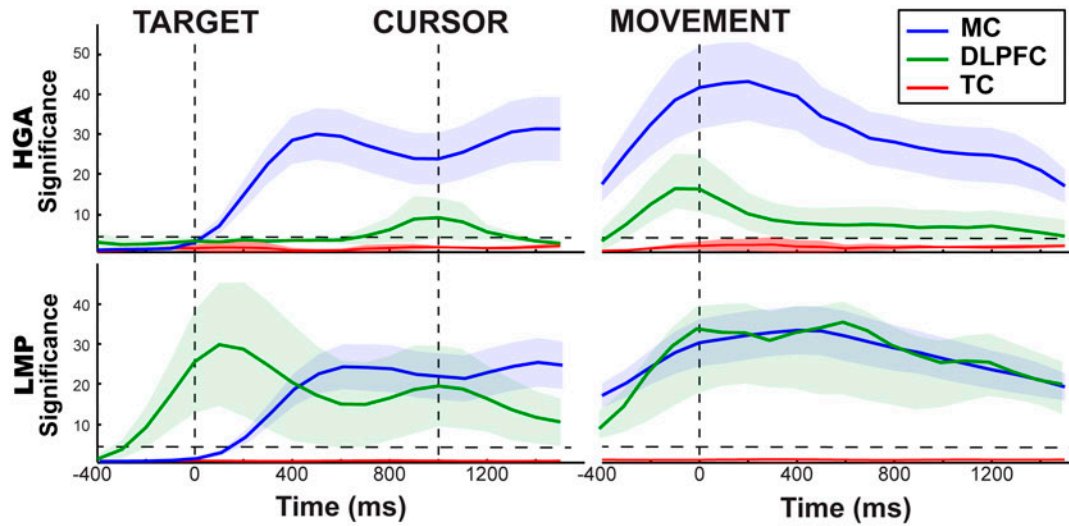
Figure 7. Temporal evolution of different cortical areas for discriminating tasks (movement preparation or execution) from rest accumulated across all subjects. Top panel: high gamma activation time aligned to target (top), cursor (middle), and movement (bottom) onsets. Bottom panel: local motor potential activation time aligned to target (top), cursor (middle), and movement (bottom) onsets. Dashed lines indicate level of statistical significance at $p = .05$.
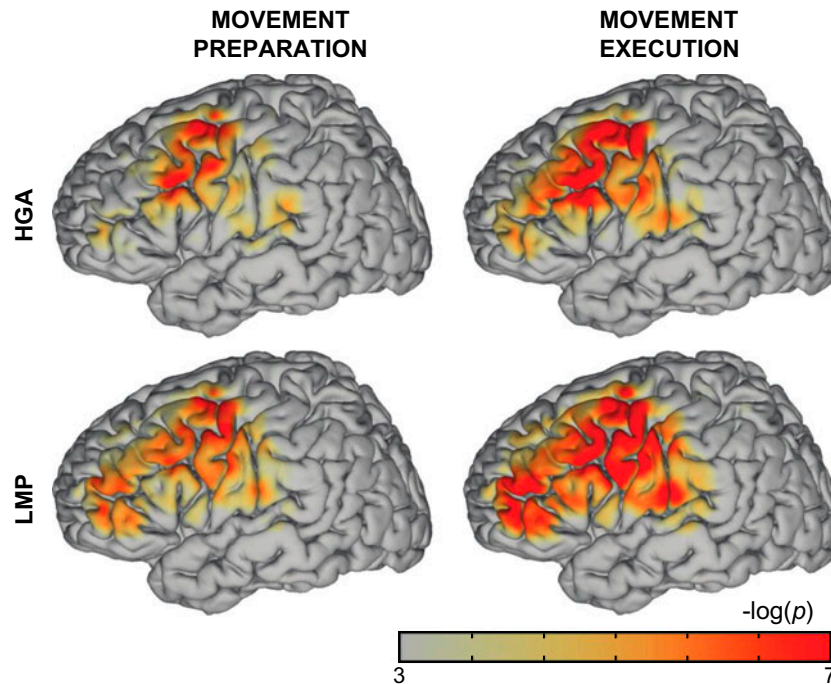

Figure 8. Cortical areas that exhibit directional tuning during intention (left column) and movement (right column) for high gamma activations (top row) and time-domain components (bottom row).

HGA is known to reflect local neural activity [16,35] and has been successfully used in real-time functional motor mapping in patients with epilepsy.[36] The changes in HGA observed in this task were temporally more discriminative between task engagement and resting state compared to narrow-banded activity in the mu or beta ranges as seen in the example mean activity in Figure 5. Moreover, in a previous study, we showed that the same HGA features could be used to faithfully predict movement onsets.[36] Note that the accumulated HGA feature activations in the top panel of Figure 6 are highly localized for activations aligned to target onset
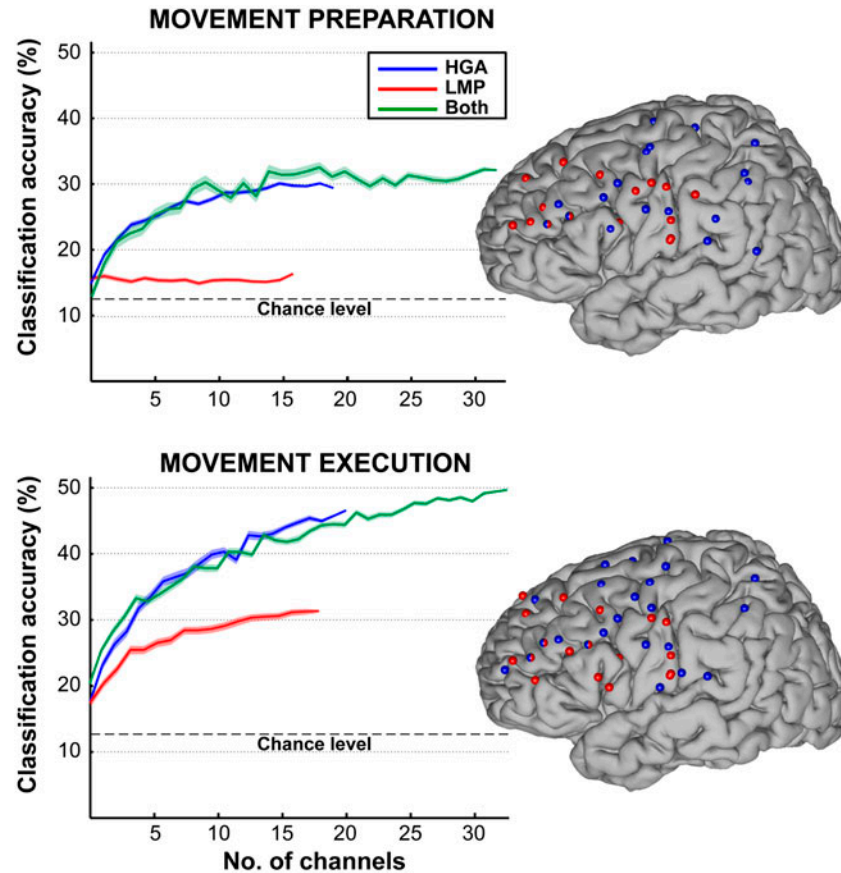
A. Gunduz et al.

Figure 9. Left: directional classification accuracies as a function of number of accumulated channels during movement preparation (top panel) and execution (bottom panel). Blue and red curves represent classification using directionally tuned channels for high gamma activity and local motor potentials, respectively. Green curves represent classification for both features. Shading around the curves denotes standard error of the means. Right: solid blue and red balls show tuned channels for HGA and LMP features. Two-colored balls represent electrodes that were tuned for both features.

Table 3. Mean magnitude of angular errors for classifying directions during movement preparation and execution.

Subject	Movement preparation		Movement execution	
	High gamma activity	Local motor potentials	High gamma activity	Local motor potentials
A	46*	55*	44*	57*
B	58*	51*	45*	51*
C	81	66	51*	63
D	65	73	53*	54*
E	62	70	53*	64
F	46*	69	46*	65
G	61	79	63	65
H	59*	64	60	51*
I	63	72	75	51*
J	60	69	59*	73
K	51*	54*	39*	

*$p < .05$.

and movement onsets (top and bottom row, respectively). When aligned around cursor presentation, the activity is broader (middle row), which is a consequence of the variance in reaction times. At 400 ms after target onset, we observe increased HGA within the premotor and parietal cortices (Brodmann areas 6 and 7, respectively), which merge over primary sensorimotor cortex at movement onset. The role of Brodmann area 7 is to guide our
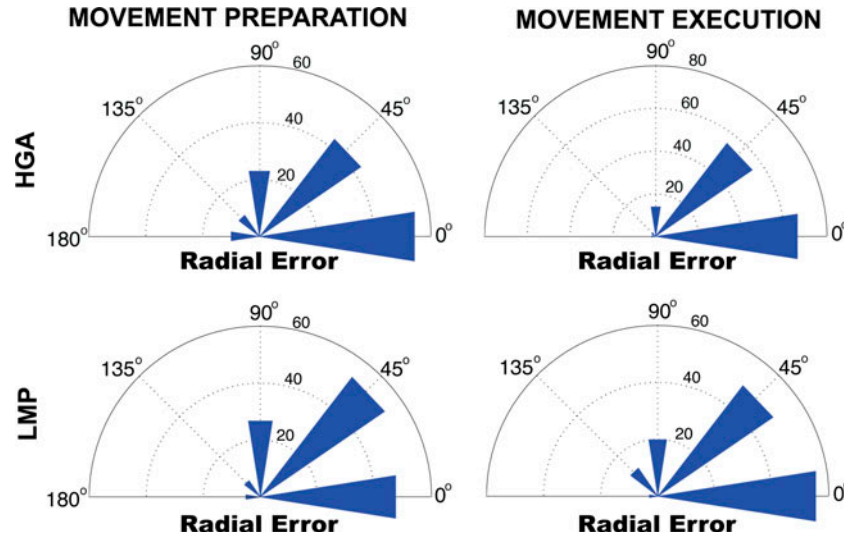
Figure 10.   Histograms of absolute classification error angles for movement preparation (left column) and execution states (right column) using all tuned HGA (top row) and LMP electrodes (bottom row). Note that 0° corresponds to accurate classification.

actions in space through proprioception.[22,37] During movement (e.g., 800 ms after movement onset), the parietal activations migrate to Brodmann area 40, which is assumed to be involved in the longer-term coding of spatial relationships, such as in delayed movements.[38–40]

Dorsolateral prefrontal cortex (Brodmann areas 9, 46) is known to be engaged in a range of aspects of cognitive control of motor behavior, such as processing sensory inputs and planning future actions.[41–43] In Figure 7, we observe that HGA in the DLPFC peaks around cursor presentation (top left in green). This suggests that this HGA is an execution-related activation in the DLPFC.[44] On the other hand, LMP activity in the DLPFC starts early on in the trial (bottom left in green), before HGA activity in the DLPFC or LMP activity in the motor cortex, suggesting it may reflect a more general process of movement preparation, such as anticipation, and only hold modest directional information (see Figure 9). Taken together, it appears quite clear that the two DLPFC activations in HGA and LMP reflect different physiological processes.

To ensure that the directional classification results in Figure 9 were not a result of small training set sizes and large number of input channels, we decreased the number of training samples by 50%. These substantially smaller sizes of the training set only very modestly reduced classification accuracies. Hence, we conclude that we have not yet reached the optimal number of input channels for the classifiers (i.e., low classification accuracies are not due to a high number of input parameters). Moreover, our analysis might be more than determining the effect of channel inclusion, but the approach also increases the heterogeneity of the inputs to the final decoding model.

In this experiment a joystick was used for the center-out task, which only requires wrist deviations compared to expansive arm reaches in typical primate center-out tasks. This small isometric motor plan and output may be the reason that the decoded directional information was not decoded in single subjects, or that the classification accuracies across the pooled channels were not high. Figure 10 shows that the most frequent directional misclassification was between a target and one of its neighbors. Hence, this small isometric movement of the joystick might have limited the resolution of the movements that could be decoded.

It should be noted that the directional classification results presented herein were based on information from electrodes that were pooled across subjects. Thus, they are not necessarily representative of results for an individual subject using a BCI. Still, our results also demonstrate that ECoG signals hold statistically significant information about movement direction in 9 of the 11 subjects. We also should point out that the directional classification results were attained in offline analyses. Nevertheless, ECoG-based BCIs have been shown to be successful in online settings (for lower dimensions or number of targets) using both LMP and HGA features.[18,19] In a previous study we showed that it is also possible to distinguish between movement preparation and execution [45] using HGA features in single trials. Moreover, BCI performance generally improves as the BCI system adapts to its user.[5,46] Classification accuracies in our task are also likely to improve with user training and reach classification accuracies of those achieved with EEG.[18,19,47]

In the context of ECoG-based decoding of directional movements as attempted in our or other studies,

the optimal electrode diameter and density remain largely undefined. Modeling studies suggest that the optimal inter-electrode distance should be in the range 1.3–1.7 mm,[48,49] and a recent study [50] demonstrated that details of hand/wrist movements can be inferred from ECoG signals recorded over motor cortex at a similar resolution (1 mm). Together with ongoing and likely future advances in miniaturization of ECoG grids and corresponding electronics,[11] this suggests that it should be possible to design small and fully implantable ECoG interfacing systems with dense electrode spacing, and that these miniaturized systems will deliver substantial information about movements. At the same time, it is becoming increasingly clear that even simple movements or other important behaviors are supported by neuronal activity in widely distributed areas of the brain,[53] and the findings from the present study suggest that sampling across these widely distributed areas provides additional information about actual or intended movements. These realities imply that there is a distinct possibility that optimization of the performance and robustness of BCI systems may require an increase in both the density and areal coverage, and thus total number of ECoG electrodes that are being sampled, but these more capable sensor designs will likely also increase clinical morbidity. In consequence, while there is encouraging initial evidence of the potential clinical relevance of ECoG-based BCI systems,[14,51,52] further delineation and eventual resolution of this important issue is likely to be of central importance to the design of clinically relevant invasive BCI devices.

Finally, the present study investigated ECoG signals during movement or movement preparation. A number of previous studies investigated movement preparation/execution along with movement imagery.[54–57]. For example, an ECoG study by Miller et al. [58] on movement imagery showed high gamma activations that were broadly distributed over sensorimotor cortex, but appeared to be more frontal compared to movement execution. The locations identified in the Miller et al. study for movement imagery are similar to those identified in our study for movement preparation.

Herein, we present evidence that movement is a complex spatiotemporal mechanism involving different distributed physiological processes that produce HGA and LMP. Thus, sampling from various areas and capturing different processes appears to be beneficial for the design of BCIs.

Disclosure statement

Funding

References

[1] Wolpaw J, Wolpaw E, *Brain-Computer Interfaces*, 1st ed. New York, NY: Oxford University Press; 2012.

[2] Broetz D, Braun C, Weber C, et al. Combination of brain-computer interface training and goal-directed physical therapy in chronic stroke: a case report. *Neurorehabil Neural Repair*. Sep. 2010; 24: 674–679.

[3] Ang KK, Guan C, Chua KSG, et al. A clinical study of motor imagery BCI performance in stroke by including calibration data from passive movement, in *Nature*. IEEE; 2013, 6603–6606.

[4] Hochberg LR, Serruya MD, Friehs GM, et al. Neuronal ensemble control of prosthetic devices by a human with tetraplegia. *Nature*. Jul 2006; 442: 164–171.

[5] Collinger JL, B Wodlinger, JE Downey, et al. High-performance neuroprosthetic control by an individual with tetraplegia. *Lancet*. Feb. 2013; 381: 557–564

[6] Rebsamen B, Guan C, Zhang H, et al. A brain controlled wheelchair to navigate in familiar environments. *IEEE Trans. Neural Syst. Rehabil. Eng.* Dec. 2010; 18: 590–598.

[7] Carlson T, Demiris Y. Collaborative Control for a Robotic Wheelchair: Evaluation of Performance, Attention, and Workload. *IEEE trans syst man cybern part B (cybern)*. Jun. 2012; 42: 876–888.

[8] Carlson T, J Del R Milla´n, Brain-Controlled Wheelchairs: A Robotic Architecture, *IEEE Rob. Autom. Mag.* 2013; 20: 65–73.

[9] Kaufmann T, Herweg A, Kubler A. Toward brain-computer interface based wheelchair control utilizing tactually-evoked event-related potentials. *J. NeuroEng.Rehabil.* 2014; 11: 7.

[10] Ball T, A Schulze-Bonhage, A Aertsen, et al. Differential representation of arm movement direction in relation to cortical anatomy and function. *J. Neural Eng.* Feb 2009; 6: 016006

[11] Schalk G, Leuthardt EC. Brain-Computer Interfaces Using Electrocorticographic Signals. *IEEE Rev. Biomed. Eng.* 2011; 4: 140–154.

[12] Chao, Long-term asynchronous decoding of arm motion using electrocorticographic signals in monkey. *Front. Neuro. Eng.* Jan 2010: 1–10.

[13] Schalk G. Can electrocorticography (ECoG) support robust and powerful brain-computer interfaces? Front. Neuro. eng. 2010; 3: 9–9.

[14] Wang W, Collinger JL, Degenhart AD, Tyler-Kabara EC, Schwartz AB, Moran DW, Weber DJ, Wodlinger B,

Vinjamuri RK, Ashmore RC, Kelly JW, Boninger ML. An electrocorticographic brain interface in an individual with tetraplegia. *PLoS One*, 2013; 8(2):e55344.

[15] Miller KJ, Honey CJ, Hermes D, et al. Broadband changes in the cortical surface potential track activation of functionally diverse neuronal populations. NeuroImage. Jan. 2014; 85: 711–720.

[16] Miller KJ, Leuthardt EC, Schalk G, et al. Spectral changes in cortical surface potentials during motor movement. J.Neurosci. Feb 2007; 27: 2424–2432.

[17] Leuthardt EC, Schalk G, Wolpaw JR, et al. A brain-computer interface using electrocorticographic signals in humans. J. Neural Eng. Jun 2004; 1: 63–71

[18] Schalk G, Miller KJ, Anderson NR, et al. Two- dimensional movement control using electrocorticographic signals in humans. J. Neural Eng. Feb 2008; 5: 75–84.

[19] Mehring C, Nawrot M, de Oliveira S, et al. Comparing information about arm movement direction in single channels of local and epicortical field potentials from monkey and human motor cortex. J. Physiology-Paris. 2004; 98: 498–506.

[20] Schalk G, Kubanek J, Miller K, et al. Decoding two-dimensional movement trajectories using electrocorticographic signals in humans. J. Neural Eng. 2007; 4: 264.

[21] Kubanek J, Miller K, et al. Decoding flexion of individual fingers using electrocorticographic signals in humans. J.Neural Eng. 2009; 6: 066001.

[22] Andersen R, Buneo C. Intentional maps in posterior parietal cortex. 2002;25:189-220. *J. Neurosci.* 2002; 25: 189–220.

[23] Bonini L, Serventi F, Simone L, et al. Grasping neurons of monkey parietal and premotor cortices encode action goals at distinct levels of abstraction during complex action sequences. J. Neurosci. 2011; 31: 5876–5886.

[24] Carmena JM, Lebedev MA, Crist RE, et al. Learning to control a brain–machine interface for reaching and grasping by primates. *J. Neurophysiol.* Nov. 2003; 1: E42.

[25] Hatsopoulos N, Joshi J, O'Leary JG. Decoding continuous and discrete motor behaviors using motor and premotor cortical ensembles. *J. Neurophysiol.* Aug 2004; 92: 1165–1174.

[26] Talairach J, Tournoux P. *IEEE Trans. Biomed. Eng.* New York, NY: Thieme Medical , Inc.; 1988.

[27] Kubanek J, Schalk G. NeuralAct: A Tool to Visualize Electrocortical (ECoG) Activity on a Three-Dimensional Model of the Cortex. *Neuroinformatics*. 2015; 13: 167–174.

[28] Lancaster JL, Woldorff MG, Parsons LM, et al. Automated talairach atlas labels for functional brain mapping. *Hum Brain Mapp*. Jul 2000; 10: 120–131.

[29] Schalk G, McFarland D, Hinterberger T, et al. BCI2000: a general-purpose brain-computer interface (BCI) system. *IEEE Trans. Biomed. Eng.* Jan 2004; 51: 1034–1043.

[30] Schalk G, Mellinger J. A Practical Guide to Brain-Computer Interfacing with BCI2000, 1st ed, Springer, London, UK, 2010.

[31] Georgopoulos AP, Schwartz AB, Kettner RE. Neuronal population coding of movement direction. *Science*. Sep 1986; 233: 1416–1419.

[32] Cogan G, Thesen T, Carlson C, et al. Sensory-motor transformations for speech occur bilaterally. *Nature*. 2014; 507: 94–98.

[33] Ritaccio A, Brunner P, Cervenka MC, et al. Proceedings of the first international workshop on advances in electrocorticography. *Epilepsy Behav*. Nov 2010; 19: 204–215.

[34] Brunner P, Ritaccio AL, Lynch TM, et al. A practical procedure for real-time functional mapping of eloquent cortex using electrocorticographic signals in humans. *Epilepsy Behav*. Jul 2009; 15: 278–286.

[35] Wang Z, Gunduz A, Brunner P, et al. Decoding onset and direction of movements using Electrocorticographic (ECoG) signals in humans. *Front. neuroeng*. 2012;5:15.

[36] Buneo C, Andersen R. The posterior parietal cortex: Sensorimotor interface for the planning and online control of visually guided movements. *Neuropsychologia*. 2006; 44: 2594–2606.

[37] WG Darling, Rizzo M, and Butler AJ. Disordered sensorimotor transformations for reaching following posterior cortical lesions. neuropsychologia 39, 237–254 (2001). *Neuropsychologia*. 2001; 39: 237–254.

[38] Milner AD, Paulignan Y, Dijkerman HC, et al. A paradoxical improvement of misreaching in optic ataxia: new evidence for two separate neural systems for visual localization. *Proc R soc London B*. 1999; 266: 2225–2229.

[39] Karnath H-O. New insights into the functions of the superior temporal cortex. *Nat. Rev. Neurosci.* 2001; 2: 568–576

[40] Boussaoud D, Barth TM, Wise SP. Effects of gaze on apparent visual responses of frontal cortex neurons. *Exp Brain Res*. Jan 1993; 93: 423–434.

[41] Funahashi S, Inoue M, Kubota K. Delay-period activity in the primate prefrontal cortex encoding multiple spatial positions and their order of presentation. *Behav. Brain Res*. 1997; 84: 203–223.

[42] Tanji J, Hoshi E. Role of the lateral prefrontal cortex in executive behavioral control. *Physiol. Rev.* 2008; 88: 37–57.

[43] Brass M, von Cramon D. The role of the frontal cortex in task preparation. *Cereb. Cortex*. 2002; 12: 908–914.

[44] Gupta D, Hill N, Brunner P, Gunduz A, Ritaccio AL, Schalk G. Simultaneous real-time monitoring of multiple cortical systems. *J. Neural Eng*. 11:056001, 2014.

[45] Milekovic T, Fischer J, Pistohl T, et al. An online brain-machine interface using decoding of movement direction from the human electrocorticogram. *J. Neural Eng.* Aug. 2012; 9: 046003.

[46] McFarland DJ, Sarnacki WA, Wolpaw JR. Electroencephalo graphic (EEG) control of three-dimensional movement. *J. Neural Eng.* 2010;7(3):036007.

[47] Freeman WJ, Rogers LJ, Holmes MD, et al. Spatial spectral analysis of human electrocorticograms including the alpha and gamma bands. *J. Neurosci. Methods*. Feb 2000; 95(2): 111–121.

[48] Slutzky MW, Jordan LR, Krieg T, et al. Optimal spacing of surface electrode arrays for brain-machine interface applications. *J. Neural Eng.* Apr 2010; 7: 026004.

[49] EC Leuthardt, Freudenberg Z, Bundy D, et al. Microscale recording from human motor cortex: implications for minimally invasive electrocorticographic brain-computer interfaces. *PLoS ONE*. Jul 2009; 27: E10.

[50] Nakanishi Y, Yanagisawa T, Shin D, et al. Prediction of Three-Dimensional Arm Trajectories Based on ECoG Signals Recorded from Human Sensorimotor Cortex. *PLoS ONE*. Aug. 2013; 8: e72085.

[51] Gharabaghi A, Naros G, Walter A, et al, "Epidural electrocorticography of phantom hand movement following long-term upper-limb amputation." *Front. human neurosci.* 2014; 8: 285.

[52] Coon WG, Gunduz A, Brunner P, et al. Oscillatory phase modulates the timing of neuronal activations and resulting behavior. *NeuroImage*, 2016; 133: 294–301.

[53] Jeannerod M. The representing brain: Neural correlates of motor intention and imagery. Behavioural Brain Research 1994;17:187–245.

[54] Sanes JN. Neurophysiology of preparation, movement and imagery. Behavioral and Brain Sciences. 1994;17: 221–223.

[55] Kranczioch C, Mathews S, Dean P, Sterr A. On the equivalence of executed and imagined movements: Evidence from lateralized motor and nonmotor potentials. Human Brain Mapping. 2009;30(10):3275–3286.

[56] Holper L, Scholkmann F, Shalom DE, Wolf M. Extension of mental preparation positively affects motor imagery as compared to motor execution: A functional near-infrared spectroscopy study. Cortex. 2012;48:593–603.

[57] Miller KJ, Schalk G, Fetz EE, den Nijs M, Ojemann JG, Rao RPN. Cortical activity during motor execution, motor imagery, and imagery-based online feedback. Proceedings of the National Academy of Sciences. 2010;107(9):4430–4435.